Modelling the electric field and the current density generated by cerebellar transcranial DC stimulation in humans

Marta Parazzini [a,*], Elena Rossi [a,c], Roberta Ferrucci [b,d], Ilaria Liorni [a,c], Alberto Priori [b,d], Paolo Ravazzani [a]

[a] CNR Consiglio Nazionale delle Ricerche, Istituto di Elettronica e di Ingegneria dell'Informazione e delle Telecomunicazioni IEIIT, Milano, Italy
[b] Dipartimento di Fisiopatologia Medico-Chirurgica e dei Trapianti, Università degli Studi di Milano, Milano, Italy
[c] Dipartimento di Elettronica, Informazione e Bioingegneria, Politecnico di Milano, Milano, Italy
[d] Centro Clinico per la Neurostimolazione, le Neurotecnologie ed i Disordini del Movimento, Fondazione IRCCS Ca' Granda Ospedale Maggiore Policlinico, Milano, Italy

Available online 28 October 2013

1. Introduction

Transcranial Direct Current Stimulation (tDCS) is a non-invasive technique that modulates brain excitability (Priori, 2003; Nitsche and Paulus, 2011; Brunoni et al., 2012). tDCS over the cerebellum (or cerebellar tDCS) influences working memory (Ferrucci et al., 2008) and the processing of negative facial emotion (Ferrucci et al., 2012), motor control (Jayaram et al., 2012), and cerebello-cerebral connections (Galea et al., 2009) in healthy subjects. Cerebellar tDCS has also been recently proposed for the treatment of cerebellar disorders (Manto, 2008).

Among the open issues concerning cerebellar tDCS, the electric current density (**J**) and the electric field (**E**) that cross the skull and

* Corresponding author. Address: Istituto di Elettronica e di Ingegneria dell'Informazione e delle Telecomunicazioni IEIIT, Consiglio Nazionale delle Ricerche, Piazza Leonardo da Vinci, 32, 20133 Milan, Italy. Tel.: +39 02 2399 3379.
E-mail address: marta.parazzini@ieiit.cnr.it (M. Parazzini).

reach the cerebellum remain unknown. We therefore aimed to evaluate the electric quantities induced within the skull by cerebellar tDCS by using computational electromagnetic techniques on three realistic human models (of different age and sex), allowing to analyze current flow through the brain, the cerebellum and the brainstem. This could be of some help particularly in the investigation about the possible involvement of the cerebral cortex during cerebellar stimulation. Moreover, this study could provide answer to possible concerns about the safety of this tDCS application, providing information about the electric field in the brainstem and the heart.

2. Methods

Simulations were conducted using the simulation platform SEMCAD X (by SPEAG, Schmid & Partner Engineering, AG, Zurich, Switzerland, www.speag.com), solving the Laplace equation to determine the electric potential (φ) distribution inside the human tissues

$$\nabla \cdot (\sigma \nabla \varphi) = 0 \quad (1)$$

where σ is the electrical conductivity of the human tissues. The **E** and **J** field distributions were obtained by means of the following relations:

$$E = -\nabla \varphi \quad (2)$$

$$J = \sigma E \quad (3)$$

Three human realistic models of the Virtual Family (Christ et al., 2010) were used. They are based on high resolution MRI of three healthy volunteers (a 26-years-old female adult model "Ella"; a 34 years-old male adult model "Duke"; an 11 years old female adolescent model "Billie") and segmented into a voxel-based format at a resolution of 1 mm. The models consist of up to 77 different tissues, the dielectric properties of which were assigned on the basis of the data at low frequency (Gabriel et al., 1996, 1997; Parazzini et al., 2011). Table 1 summarizes the conductivities assigned to the different tissues.

The active electrode was placed on the scalp over the cerebellar area (approximately centred on the median line 2 cm below the inion with its lateral borders about 1 cm medially to the mastoid apophysis) and the reference over the right arm as reported elsewhere (Ferrucci et al., 2008, 2012). The electrodes were modeled as rectangular pads conductors (σ = 5.9 × 10^7 S/m) of 5 × 7 cm^2 placed above a rectangular sponge (σ = 0.3 S/m) of 7 × 8 cm^2, as used in clinical practice. The potential difference between the elec-trodes was adjusted to inject a total current of 2 mA. The current value was computed by integrating the current density on the wires surfaces attached to the electrodes (note that the wires are not shown in the following Fig. 1). It resulted in an average potential difference of about 1.2 V across the models. For each simulation, the human model and the electrodes were inserted in a surrounding bounding box filled with air. The boundaries of the bounding box were treated as insulated, i.e., the normal component of the current density was set equal to zero ($J \cdot n = 0$). Continu-ity of the tangential component of **E** was applied at each tissue-to-tissue boundary ($E_{t1} = E_{t2}$; which is equivalent to $J_{t1}/\sigma_1 = J_{t2}/\sigma_2$). At the interface between the skin and the air the current density was set to be parallel to the face (Parazzini et al., 2011, 2012).

The spatial amplitude distribution of **E** and **J** was analyzed in different brain regions, such as the cerebellum, the cortex, the white matter, the medulla oblongata, the pons, the midbrain, and the thalamus. Moreover, since the reference electrode is placed extracephalic on the right arm, these distributions were also evaluated in the heart. Descriptive statistics of the **E** and **J**-field amplitudes (median, 25th and 75th percentiles, minimum and maximum) in the brain and heart were then computed. The maximum of the amplitude distribution was identified as its 99th percentile. This was used instead of the maximum to take into account possible computational instabilities (Parazzini et al., 2011, 2012). In the following, we will use the word "peak" or "maximum" for the 99th percentile of the distribution.

Table 1
Conductivities assigned to the different tissues.

Tissues	Conductivity (S/m)
Adrenal gland, epididymis, hypophysis, pancreas, stomach, stomach lumen, small intestine, small intestine lumen, thymus, thyroid gland	0.51113
Air internal, pharynx, trachea lumen	0
Artery, vein, blood vessel, penis	0.7
Bladder	0.202783
Bone, mandible, marrow red, patella, skull, teeth, vertebrae	0.020028
Brain grey matter, hippocampus, hypothalamus, pineal body, thalamus	0.027512
Brain white matter, commissura anterior, commissura posterior	0.027656
Breast	0.2617535
Bronchi, bronchi lumen	0.250552
Cartilage, ear cartilage, intervertebral disk, larynx, meniscus, trachea	0.16113
Cerebellum	0.047512
Cerebro spinal fluid	2
Connective tissue	0.1215635
Cornea	0.4113
Diaphragm, muscle	0.201967
Ear-skin, skin	0.012147
Esophagus, esophagus-lumen	0.51113
Eye lens, ovary	0.3113
Eye sclera	0.501392
Eye vitreous humor	1.5
Fat, Subcutaneous Adipose Tissues (SAT)	0.012207
Gallbladder	0.9
Heart lumen	0.7
Heart muscle	0.053677
Kidney cortex, kidney medulla	0.0544105
Large intestine, large intestine lumen	0.0122052
Liver	0.027714
Lung	0.120847
Medulla oblongata, midbrain, pons	0.027584
Mucosa	0.0004
Nerve, spinal cord	0.017126
Prostate, testis	0.41113
Spleen	0.0395962
Tendon ligament	0.250922
Tongue	0.26113
Ureter-urethra	0.25055
Uterus	0.201296
Vagina	0.0122052

To assess whether and how the **E** and **J** fields depended on the exact electrode placement, systematic changes in the positioning of the active electrode were performed on the model "Ella". Specifically, the active electrode was moved longitudinally and laterally by ±1 cm. Fig. 1 shows a back view of the electrodes positioning during cerebellar tDCS (Fig. 1A where the model "Ella" was used as example) and a sagittal plane through the same model showing the electrode–skin interface and the anatomical details of the mod-el itself (Fig. 1B).

3. Results

The higher **J**-field amplitudes generated by cerebellar tDCS were near the active electrode in the cerebellum at cortical level within the posterior lobe (Fig. 2). The **J** spread over the occipital cortex – quantified as the percentage of occipital volume where the amplitude of **J**-field is greater than 70% of the peak of **J** in the cerebellum

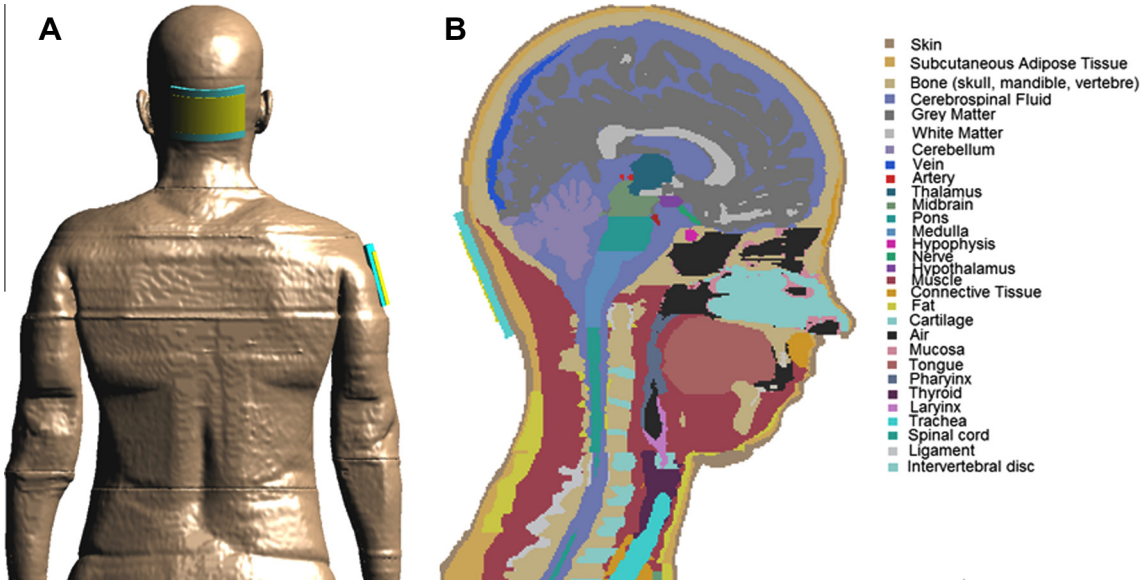

Fig. 1. (A) Back view of the electrodes positioning for "Ella" (here used as an example); the yellow rectangular pad is the conductor, while the light blue rectangular pad is the sponge. Here the sponge is in contact with the skin of the arm for about 70% of its surface area (about 39.2 cm^2). (B) Sagittal plane through "Ella" showing the electrode–skin interface and the anatomical detail of the human model. The legend shows the correspondence between the segmentation colors and the tissues. (For interpretation of the references to colour in this figure legend, the reader is referred to the web version of this article.)

– was only 4% for "Duke" and much less than 1% for "Ella" and "Billie". The **J** slightly spreads also to the more anterior area of the cerebellum, particularly in the adolescent "Billie", where the **J**-field amplitude distribution was less focal (Fig. 3). Indeed, whereas the percentage of volume of the cerebellum where the amplitude of **J**-field is greater than 70% of its peak was comparable with the one obtained in the adult models, the percentage of volume where the amplitude of **J**-field is greater than 50% of its peak is 2.5 times higher than that in the adult models and was 27.2%. Therefore, "Billie" shows a more widespread **J**-field amplitude distribution in the cerebellum.

Though **E**-(left panel) and **J**-(right panel) fields evaluated as average across the models were maximum in the cerebellum, marginally they spread also to other brain structures, apart from the occipital cortex (Fig. 4, first row). Particularly, the medians of **E** and **J** in the other brain structures were reduced with respect to those in the cerebellum of an amount that ranged from about 44% (in the medulla) to 78% (in the white matter) and from 68%(in the medulla) to 87% (in the white matter), for **E** and **J**, respectively.

The analysis of **J** and **E** averaged across the models found peaks of the amplitude spatial distributions of **E** and **J** in the heart of 0.66 V/m and 0.04 A/m^2.

The anthropometric variables of the subject, his/her morphology and anatomical characteristics turn out in distinct field amplitude distributions (Figs. 2 and 4, from second to fourth row). However, the pattern of these distributions across the different structures is qualitatively comparable. For example, compared to the median values observed in the cerebellum, the medians of **E** (Fig. 4, left column) were reduced of an amount that ranged from 46% (in the medulla) to 86% (in the white matter) for "Ella", from 48% (in the medulla) to 77% (in the white matter) for "Billie" and from 32% (in the medulla) to 71% (in the thalamus) for "Duke". The median values of **J**-field amplitude distributions (Fig. 4, right column) were remarkably higher in the cerebellum than in other cortical or subcortical structures: the smallest reductions were observed in "Duke" where the reduction of the median of **J** with respect to the cerebellum ranged from 61% (in the medulla) to 83%(in the thalamus).

Finally, changes by ±1 cm in the placement of the active electrode turned out in a small effect on the field amplitude distributions (Fig. 5). This could suggest an important role of the 3D-complex anatomical structures of the human body on the field amplitude distribution, which could not be easily inferred only from simple consideration on the relative position between the electrode and the structure itself (i.e. a possible shift toward right and toward left of the field amplitude distribution according to the electrode movement). Therefore, the influence of the cerebellum shape and anatomy seems to be higher than the effect of the electrode shift. In particular, the **J** spread over the occipital cortex remains always less than 1%, as before for the same human model. Moreover, changing the electrode position, the maximum difference among the percentage of volume of the cerebellum where the amplitude of **J**-field is greater than 70% of its peak is less than 1% (with the higher value when the active electrode is moved longitudinally in the down direction). Moreover, the maximum difference among the percentage of volume where the amplitude of **J**-field is greater than 50% of its peak is about 4%, with the higher spread toward the more anterior part of the cerebellum when the active electrode is moved longitudinally toward the anion (i.e., in the up direction). As to the variation of the amplitude of the current density in the cerebellum due to the change of the ac-tive electrode position, the ratio between the standard deviation and the mean (i.e., the coefficient of variability) of the **J** peak values in the cerebellum is 8%.

4. Discussions and conclusions

We here reported the first modeling study on the electric field generated by transcutaneous cerebellar DC stimulation in humans. Despite some inter-individual differences, cerebellar tDCS generates the highest electric field and current density below the stimulating electrode in the posterior cerebellum with a slight spread to other structures (Fig. 2). Within the cerebellum the current density distribution varies across different subjects, being maximum toward the more anterior part in the youngest model (Fig. 3). This observation could be particularly useful in the clinical application of cerebellar tDCS in children and adolescents, since, for these

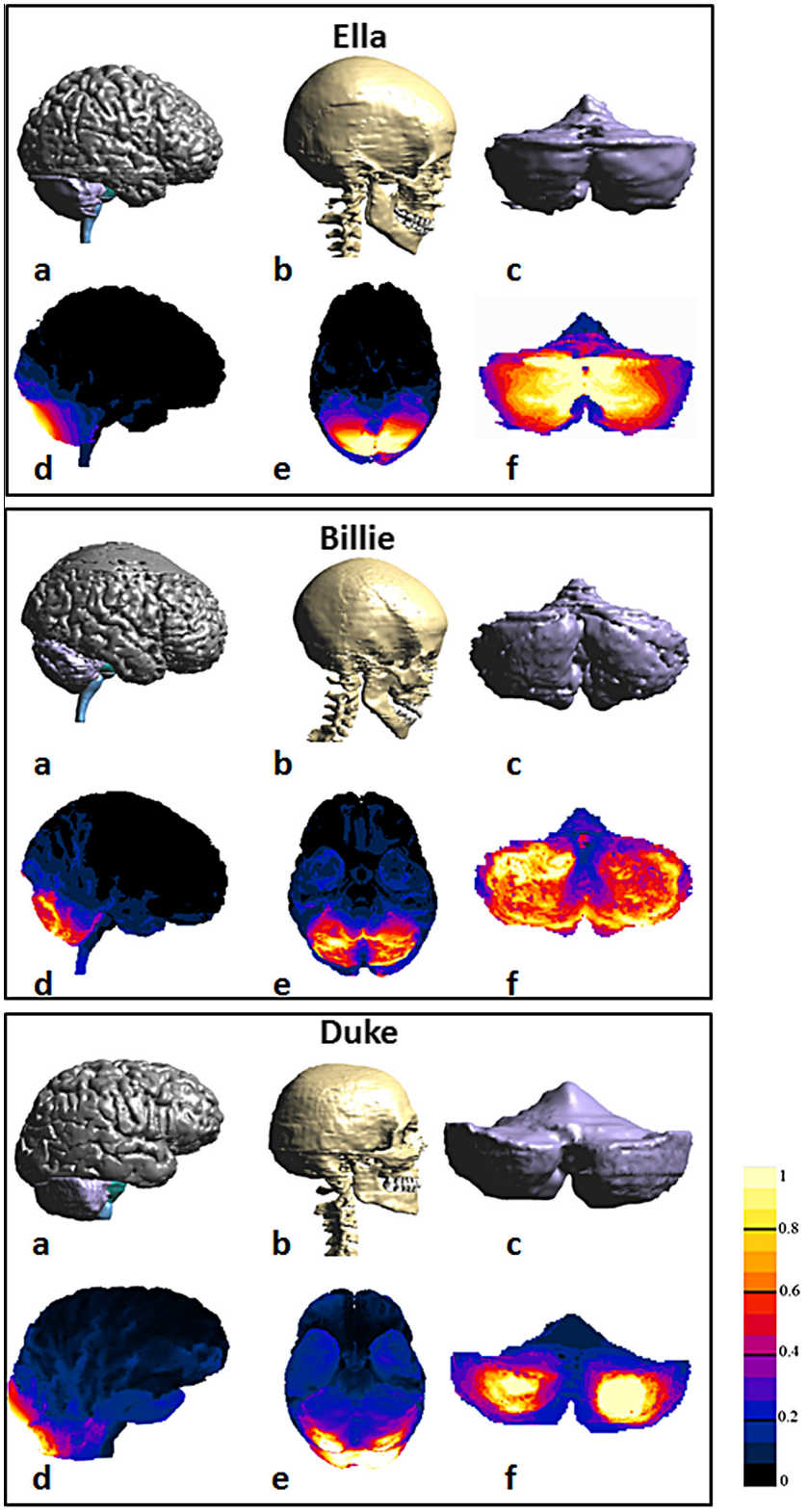

Fig. 2. Segmentation masks for "Ella" (top row), "Billie" (middle row) and "Duke" (bottom row); (a) lateral view of grey matter, cerebellum, pons, midbrain, medulla; (b) lateral view of skull (minimum skull thickness at the cerebellar level: 5 mm for "Ella"; 3 mm for "Billie"; 6 mm for "Duke"); (c) back view of cerebellum. Lateral (d) and inferior (e) views of current density amplitude field distributions over cortical, subcortical and brain-stem regions across all models; (f) back view of current density amplitude field distributions over the cerebellum. The values are normalized with respect to the maximum of the current density amplitude in the cerebellum (0.21 A/m^2, 0.16 A/m^2, 0.13 A/m^2 for "Ella", "Billie" and "Duke", respectively).

subjects, it could be possible to reach more anterior parts of the cerebellum. This is important since an activation likelihood estimate meta-analysis of neuroimaging studies (Stoodley and Schmahmann, 2009) has provided support for an anterior sensorimotor vs. posterior cognitive/emotional dichotomy in the human cerebellum.

In all models, outside the cerebellum, the current spreading to other anatomical structures is negligible and unlikely to produce

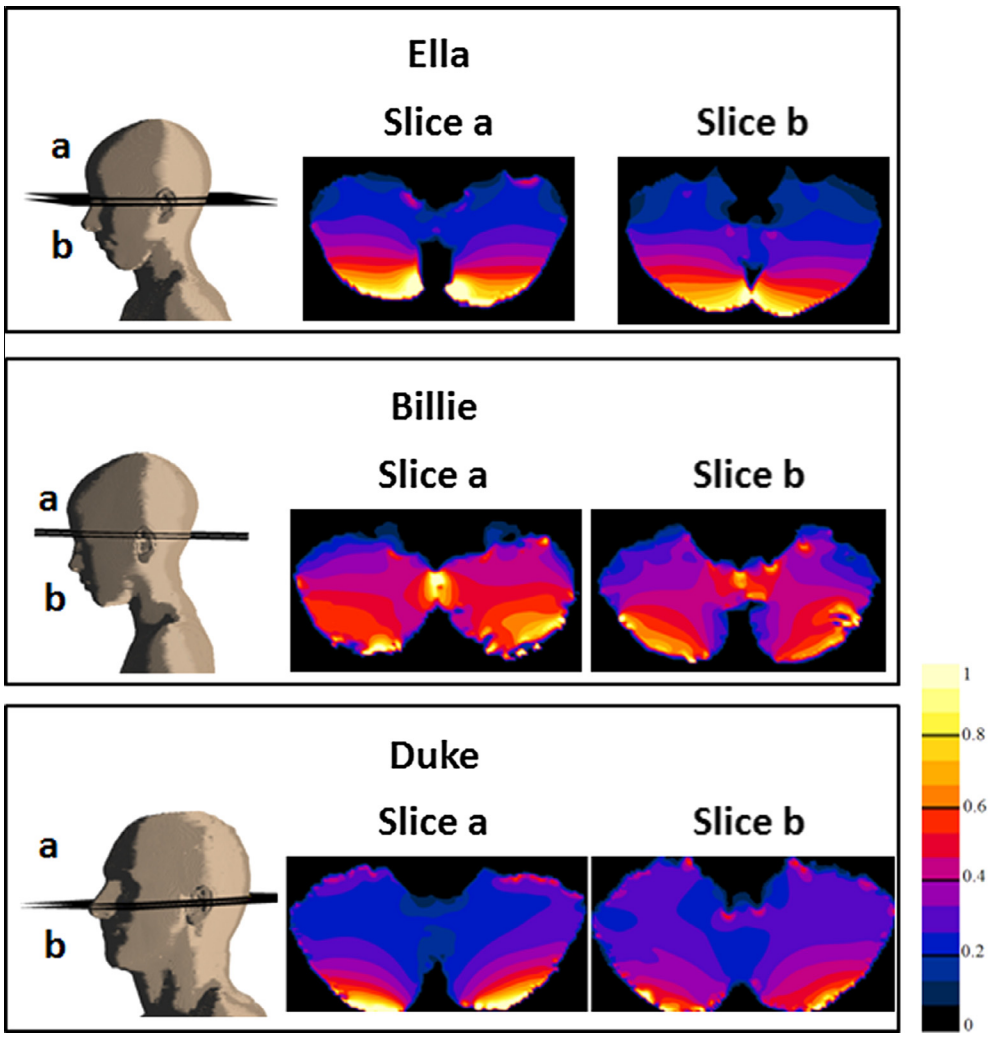

Fig. 3. Transversal sections across the cerebellum of the current density amplitude distributions for "Ella" (top row), "Billie" (middle row) and "Duke" (bottom row). The first column on the left shows for each subject transversal planes where the sections were calculated. The values are normalized with respect to the maximum of the current density amplitude in the cerebellum (see Fig. 2). Note the slight spread of **J**-field toward the more anterior area of the cerebellum particularly for the adolescent "Billie".

functional effects. This conclusion is in line with previous experimental observations that cerebellar tDCS failed to influence visual evoked potentials (Ferrucci et al., 2008) excluding, therefore, a direct stimulation of the visual cortex.

Finally, small changes in the active electrode position turn out in a negligible effect (i.e., less than 4%) on the spatial amplitude distributions (Fig. 5) and on the amplitude value (i.e., a coefficient of variation of the peak of 8%). This suggests that fine placement of the stimulating electrode does not influence so much the current density in the cerebellum and in the occipital cortex, and hence sophisticated neuronavigation systems are not specifically required for cerebellar tDCS, further supporting the simplicity and easy applicability of the technique.

In conclusion, our modeling study confirms that the cerebellum is the structure mainly involved by cerebellar tDCS. This conclusion is consistent with several biological observations. At the scalp site for cerebellar tDCS, the cerebellum is more superficial than, for in-stance, the motor cortex below the fronto-parietal bone (Axelsson et al., 2005). Also, the impedance of neural elements in the cerebellar cortex is lower than that of elements in the motor cortex. For instance, in the rat, input impedance of Purkinje cells is about one third of that of pyramidal cells in the motor cortex or of the neurons in layers 4 or 2/3 of the primary visual cortex (Zhu et al., 2006; Jacobson et al., 2005; Desai et al., 2002), leading to larger current flow through the cell membrane of Purkinje cells in the cerebellar cortex than through the neurons in the cerebral cortex.

Our results show that individual anatomical variability somehow influences the field distribution. Interestingly, the variability in the field distributions due to the use of different human models is higher than the one due to the variation of the electrode position. This is as expected and also in line with previous study (Parazzini et al., 2012), bearing in mind the great difference in size and geometry among the head models. For example, "Duke" presents a higher spread of the field amplitude toward the occipital region of the cortex compared to the other models. The differences in the cerebrospinal fluid distribution and/or in the skull thickness among the models could explain this spread (Bikson et al., 2012).

Our findings do not support the hypothesis that cerebellar tDCS significantly spreads to the brainstem. This conclusion is in line with another study (Galea et al., 2009) that showed that cerebellar tDCS at 2 mA did not alter brainstem excitability. Moreover, the values found in the pons and the midbrain agree with our previous estimation (Parazzini et al., 2013a) showing that tDCS with an extracephalic reference electrode is not relevant at the level of the brainstem. Finally, still concerning safety, the current spread to the heart is low. The values obtained in our models agree with those obtained by our group with the same modeling approach but using a different electrodes montage (Parazzini et al., 2013b).

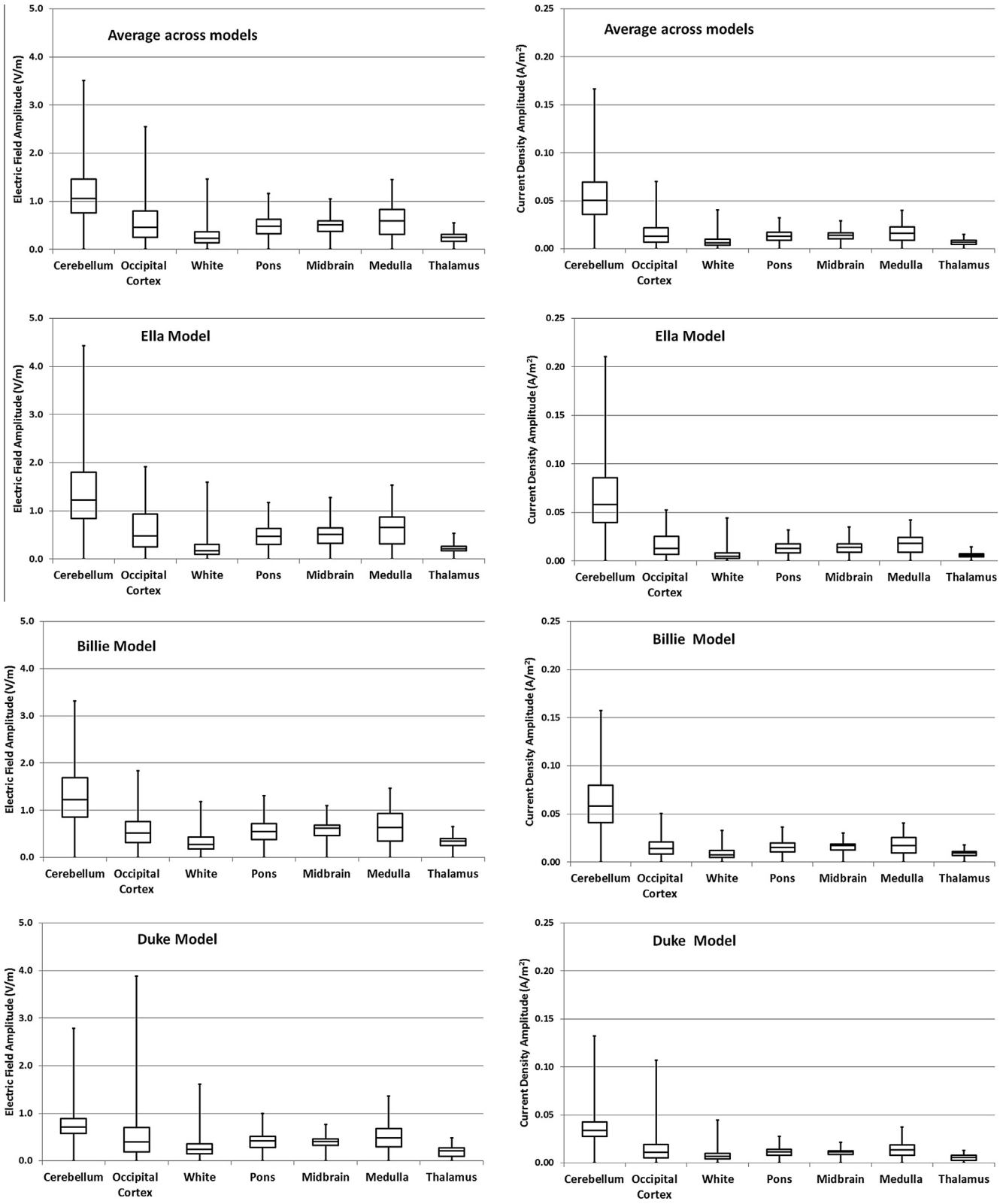

Fig. 4. Descriptive statistics of electric field (left column) and current density (right column) amplitude distribution in different brain tissues averaged across the three human models (first row) and for each human model, "Ella" (second row), "Billie" (third row) and "Duke" (bottom row). In each panel, the boxes indicate the interquartile range (25^{th}–75th percentile) with the median marked by thick horizontal black line. The whiskers delimit the minimum and maximum of the field distributions in the specific brain region.

Experimental validation of **E**- (and -**J**) amplitude estimations by numerical computation remains a challenging problem due to the unavailability of methods for high resolution in vivo **E**-field measurements (Lee et al., 2012). Nevertheless, the median values of the fields estimated in this study in the brain tissues are in agreement with some modeling studies (e.g. Sadleir et al., 2010; Lee

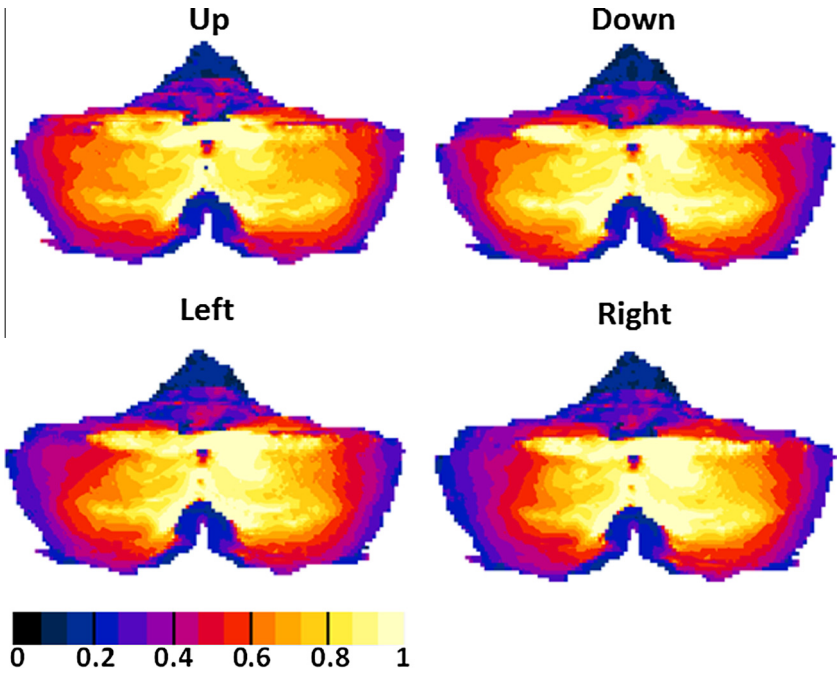

Fig. 5. Current density amplitude field distributions over the cerebellum for "Ella" when the active electrode was moved longitudinally (up and down) and laterally (left and right) by ±1 cm. The values are normalized with respect to the maximum of the current density amplitude in the cerebellum found in the model "Ella" when the active electrode is not moved (0.21 A/m^2).

et al., 2012; Parazzini et al., 2011, 2012), whereas the peak values are higher than those ones published by some others (e.g., Datta et al., 2009, 2011; Miranda et al., 2013), often the only reported statistics in the papers. This discrepancy was also found in other validations, based on the comparison with previously published studies (see, for example, Lee et al., 2012). The main reasons of those differences are in the various approaches, in terms of methods and parameters, applied in the various studies. Very high differences can be found when the studies differ, for example, in the used models (e.g., geometrical models with spheres versus realistic models from MRI images and/or different MRI-derived models), in the head and/or brain tissues considered (in terms of both type and number of tissues), in the set of dielectric properties applied. Studying this issue in TMS, Thielscher and colleagues (Thielscher et al., 2011), for example, found about a 51% of increase of the maximum **E**-field strength when anatomically-realistic model are compared to spherical ones. Moreover, as there is no standard protocol for tissue imaging or segmentation, also diversity in the segmented tissue masks will invariably influence predicted current flow (Bikson and Datta, 2012). When an anatomically realistic model is discretized, an intrinsic level of uncertainty due to numerical artifacts, which are introduced, for example, by the grid resolution, should always be considered. This especially influences the prediction of the peak values (Chen et al., 2013). Last but not least, the published studies often address different tDCS electrode montages, thus generating different field distributions. All these considerations make therefore difficult a comparisons of the results among different studies. This is even truer for the present study, which is, at least to our knowledge, the first one that investigates the distribution of the fields generated by cerebellar tDCS.

From a quantitative point of view, the comparison between the field values in this study and the results of some other investigations (e.g., Datta et al., 2009, 2011; Miranda et al., 2013) turns out in non-negligible peak differences. The comparative analysis of the approaches in terms of modeling and the consideration about the fact that the electric field is the quantity showing the largest differences, brings us to identify the main origin of these differences in the set of tissue dielectric properties applied. In this study, consistently with previous studies of the same group of authors, the set of dielectric properties to be used was identified in the database proposed by Gabriel and colleagues (Gabriel et al., 1996, 1997), with the exception of the skin (Parazzini et al., 2011). The Gabriel database includes the dielectric properties of a large number of biological tissues (about 57 in the original ver-sion) as a function of the frequency from 10 Hz to 100 GHz and, to our knowledge, it is the most complete database of the dielectric properties of biological tissues available in literature. Not secondary in our choice is also the practical consideration that, in our case in which the model is based on up to 77 tissues, only the Gabriel database allows us to be consistent among tissues in the setting their dielectric properties, using conductivity data, collected using similar experimental procedures. This, for example, allows the use of the dielectric conductivity for the cerebellum, available in the Gabriel database, instead of a value obtained as a mixture of the grey and the white matter. As drawback of the choice, the Gabriel database provides the data only starting from a minimum frequency of 10 Hz, and hence, these values are used as surrogate for the case of static fields, such as in tDCS. Our choice, therefore, differs from those ones of other authors (e.g., Datta et al., 2009, 2011; Miranda et al., 2013), who used conductivity values derived from different static resistivity measures, available only for a very limited number of tissues. The use of these values instead of those extrapolated from 10 Hz data, as we did, is still an outstanding issue (Bikson et al., 2012).

As to other limitations of the modeling procedure applied here, one should take into account that the appropriate incorporation of the tissue anisotropy (from diffusion tensor imaging) would increase the model precision. As to the geometrical structure of the models, the tissue masks are not always an exact representation of the real head. For example in all the models but with high variability across the models, there are some points in which the thickness of the CSF, filling the space between the brain and the skull, is lower than the grid resolution, leading to a direct contact

between the brain and the skull. On the contrary, apart from the inclusion of a higher number of tissues, there are other geometrical improvements of our models compared to other published models, e.g., that the head is not truncated (see for example Miranda et al., 2013) and the torso is not modeled as a synthetic region (see, for example, Datta et al., 2011) but it is a realistic torso MRI-derived.

In conclusion, even if with some limitations and shortcomings, the modeling approach used in this study is adequate to sustain the conclusions drawn in this study.

Financial disclosures

Prof. Alberto Priori and Dr. Roberta Ferrucci reports no financial interests or potential conflicts of interests; Roberta Ferrucci and Alberto Priori are stakeholders of Newronika s.r.l., a spin-off company of the Fondazione IRCCS Ca' Granda Ospedale Maggiore Policlinico and of the Università degli Studi di Milano.

Acknowledgment

The authors wish to thank Schmid & Partner Engineering AG (www.speag.com) for having provided the simulation software SEMCAD X.

References

Axelsson S, Kjaer I, Heiberg A, Bjornland T, Storhaug K. Neurocranial morphology and growth in Williams syndrome. Eur J Orthod 2005;27:32–47.

Bikson M, Rahman A, Datta A, Fregni F, Merabet L. High-resolution modeling assisted design of customized and individualized transcranial direct current stimulation protocols. Neuromodulation 2012;15:306–15.

Bikson M, Datta A. Guidelines for precise and accurate computational models of tDCS. Brain Stimul 2012;5:430–1.

Brunoni AR, Nitsche MA, Bolognini N, Bikson M, Wagner T, Merabet L, et al. Clinical research with transcranial direct current stimulation (tDCS): challenges and future directions. Brain Stimul 2012;5:175–95.

Chen XL, Benkler S, Chavannes N, De Santis V, Bakker J, van Rhoon G, et al. Analysis of human brain exposure to low-frequency magnetic fields: a numerical assessment of spatially averaged electric fields and exposure limits. Bioelectromagnetics 2013;34:375–84.

Christ A, Kainz W, Hahn GE, Honegger K, Zefferer M, Neufeld E, et al. The Virtual Family-development of surface-based anatomical models of two adults and two children for dosimetric simulations. Phys Med Biol 2010;55:N23–38.

Datta A, Bansal V, Diaz J, Patel J, Reato D, Bikson M. Gyri-precise head model of transcranial direct current stimulation: improved spatial focality using a ring electrode versus conventional rectangular pad. Brain Stimul 2009;2:201–7.

Datta A, Baker JM, Bikson M, Fridriksson J. Individualized model predicts brain current flow during transcranial direct-current stimulation treatment in responsive stroke patient. Brain Stimul 2011;4:169–74.

Desai NS, Cudmore RH, Nelson SB, Turrigiano GG. Critical periods for experience-dependent synaptic scaling in visual cortex. Nat Neurosci. 2002;5:783–9. Ferrucci R, Giannicola G, Rosa M, Fumagalli M, Boggio PS, Hallett M, et al. Cerebellum and processing of negative facial emotions: cerebellar transcranial DC stimulation specifically enhances the emotional recognition of facial anger and sadness. Cogn Emot 2012;26:786–99.

Ferrucci R, Marceglia S, Vergari M, Cogiamanian F, Mrakic-Sposta S, Mameli F, et al. Cerebellar transcranial direct current stimulation impairs the practice-dependent proficiency increase in working memory. J Cogn Neurosci 2008;20:1687–97.

Gabriel S, Lau RW, Gabriel C. The dielectric properties of biological tissues: II. Measurements in the frequency range 10 Hz to 20 GHz. Phys Med Biol 1996;41:2251–69.

Gabriel C. Comments on dielectric properties of the skin. Phys. Med. Biol. 1997;42:1671–4.

Galea JM, Jayaram G, Ajagbe L, Celnik P. Modulation of cerebellar excitability by polarity-specific noninvasive direct current stimulation. J Neurosci 2009;29:9115–22.

Jacobson GA, Diba K, Yaron-Jakoubovitch A, Oz Y, Koch C, Segev I, et al. Subthreshold voltage noise of rat neocortical pyramidal neurones. J Physiol 2005;564:145–60.

Jayaram G, Tang B, Pallegadda R, Vasudevan EV, Celnik P, Bastian A. Modulating locomotor adaptation with cerebellar stimulation. J Neurophysiol 2012;107:2950–7.

Lee WH, Deng ZD, Kim TS, Laine AF, Lisanby SH, Peterchev AV. Regional electric field induced by electroconvulsive therapy in a realistic finite element head model: influence of white matter anisotropic conductivity. Neuroimage 2012;59:2110–23.

Manto A, Ben Taib NO. A novel approach for treating cerebellar ataxias. Med Hypotheses 2008;71:58–60.

Miranda PC, Mekonnen A, Salvador R, Ruffini G. The electric field in the cortex during transcranial current stimulation. Neuroimage 2013;70:48–58.

Nitsche MA, Paulus W. Transcranial direct current stimulation-update 2011. Restor Neurol Neurosci 2011;29:463–92.

Parazzini M, Fiocchi S, Rossi E, Paglialonga A, Ravazzani P. Transcranial direct current stimulation: estimation of the electric field and of the current density in an anatomical human head model. IEEE Trans Biomed Eng 2011;58:1773–80. Parazzini M, Fiocchi S, Ravazzani P. Electric field and current density distribution in an anatomical head model during transcranial direct current stimulation for tinnitus treatment. Bioelectromagnetics 2012;33:476–87.

Parazzini M, Rossi E, Rossi L, Priori A, Ravazzani P. Evaluation of the current density in the brainstem during transcranial direct current stimulation with extra-cephalic reference electrode. Clin Neurophysiol 2013a;124:1039–40. Parazzini M, Rossi E, Rossi L, Priori A, Ravazzani P. Numerical estimation of the current density in the heart during transcranial direct current stimulation. Brain Stimul 2013b;6:457–9.

Priori A. Brain polarization in humans: a reappraisal of an old tool for prolonged non-invasive modulation of brain excitability. Clin Neurophysiol 2003;114:589–95.

Sadleir RJ, Vannorsdall TD, Schretlen DJ, Gordon B. Transcranial direct current stimulation (tDCS) in a realistic head model. Neuroimage 2010;51:1310–8.

Stoodley CJ, Schmahmann JD. Functional topography in the human cerebellum: a meta-analysis of neuroimaging studies. Neuroimage 2009;44:489–501. Thielscher A, Opitz A, Windhoff M. Impact of the gyral geometry on the electric field induced by transcranial magnetic stimulation. Neuroimage 2011;54:234–43. Zhu L, Scelfo B, Tempia F, Sacchetti B, Strata P. Membrane excitability and fear conditioning in cerebellar Purkinje cell. Neuroscience 2006;140:801–10.